A fully implicit plasticity model for the characterization of ceramics in ballistic protection

Simons, Erik; Weerheijm, Jaap; Sluijs, Bert

Publication date
2016

Document Version
Accepted author manuscript

Published in
22nd Technical Meeting DYMAT 'Experimental Testing and Modelling of Brittle Materials at High Strain-Rates'

Citation (APA)
Simons, E., Weerheijm, J., & Sluijs, B. (2016). A fully implicit plasticity model for the characterization of ceramics in ballistic protection. In *22nd Technical Meeting DYMAT 'Experimental Testing and Modelling of Brittle Materials at High Strain-Rates': Grenoble, France* (pp. 17-22)

Important note
To cite this publication, please use the final published version (if applicable).
Please check the document version above.

A Fully Implicit Plasticity Model for the Characterization of Ceramics in Ballistic Protection

E. C. Simons*†, J. Weerheijm, L. J. Sluys

Delft University of Technology, P.O. Box 5048, 2600 GA Delft, The Netherlands

Keywords: Ceramic, Indentation, JH2, quasi-static, implicit

Abstract

The Johnson-Holmquist-2 ceramic model is used for quasi-static indentation simulation. A modification is proposed to an associated plasticity formulation. This allows for a fully implicit solution scheme, where dilatation is used instead of the traditional explicit bulking formulation. Dilatation is shown to have an important influence on ring-crack formation during indentation. A mesh refinement study is performed to show the current tensile failure behaviour leads to mesh-dependent results.

Introduction

For dynamic impact simulation of ceramics the models by Johnson-Holmquist (JH1 [1], JH2 [2]) and Johnson-Holmquist-Beissel (JHB [3]) are often used. Parameters for these models can be obtained through dynamic experiments. Parameters such as material strength and stiffness are relatively easily calibrated to experiments. However measuring quantities such as damage growth and strength degradation remains difficult, due to the very high rates, catastrophic failure and their localized appearance. Often these damage related parameters and formulations are obtained through inverse modelling.

Quasi-static indentation testing of ceramics yields additional information to dynamic testing. Indentation tests allow for a controlled failure of the material and provide valuable information on ceramic failure phenomena. Although quasi-static indentation lacks dynamic effects, similarities in stress conditions between the first moments of impact and quasi-static indentation are widely recognized [4,5,6].

Calibrating ceramic material models on indentation tests can be done with finite element method (FEM) simulations. Implicit solution algorithms can be used for these quasi-static simulations. Compared to explicit algorithms large loading steps are possible and step size dependence is absent. However, in order to reap full benefits of the implicit method, a consistent tangent needs to be constructed by linearizing the constitutive relations. For the JH material model this is a non-trivial task, as it holds many non-linear relations. Furthermore, the JH bulking formulation is explicit in nature and hence cannot be used in an implicit formulation. An alternative formulation based on associated plasticity is proposed which does allow an implicit formulation, while results similar to bulking can be obtained.

The JH2 material model is a softening plasticity model. These type of material models are known to give mesh dependent results and are prone to localization. In the last part of the paper a mesh-refinement study will be performed..

*Author for correspondence (E.C.Simons@tudelft.nl).
†Present address: Delft University of Technology, P.O. Box 5048, 2600 GA Delft, The Netherlands

Methods and Models

Simulation of indentation on ceramics is done using the FEM. Unit tests are performed in a plane-strain formulation, indentation simulations are performed in an axi-symmetric formulation. Contact between indentor and ceramic is described by a penalty formulation with stick-slip frictional contact, and linearized to obtain its consistent tangent contribution [7]. A converged stress state and consistent tangent for the indentor and target material are obtained through an Euler Backward scheme with a Newton-Raphson loop on integration point level [8]. Global equilibrium is obtained using the consistent tangent with a global Newton-Raphson scheme.

Standard JH2 material model

For the Johnson-Holmquist 2 material model the yield function reads

$$f(I_1, J_2, D) = \sigma_{eq}(J_2) - \sigma_y(I_1, D), \qquad \textbf{Equation 1}$$

in which I_1 and J_2 are stress invariants and $D \in [0..1]$ is a scalar damage variable. The yield stress σ_y for JH2 is found as

$$\sigma^*_y(I_1, D) = (1 - D)\,\sigma_i^*(I_1) + D\sigma_f^*(I_1), \qquad \textbf{Equation 2}$$

where the superscript $*$ indicates that the stress values are normalized with respect to the Hugoniot elastic limit σ_{HEL} and the subscripts i and f relate to the intact and failed (i.e. residual) material strengths. Von Mises equivalent stress $\sigma_{eq} = \sqrt{3J_2}$ is used in Equation 1. Plastic deformation is obtained through the flow rule $\dot{\boldsymbol{\epsilon}}_p = \dot{\lambda}\,\partial g/\partial \boldsymbol{\sigma}$, where the plastic potential function

$$g(J_2, D) = \sigma_{eq}(J_2) = \sqrt{3J_2}. \qquad \textbf{Equation 3}$$

For this plastic potential function it can be shown that the volumetric plastic strain $\epsilon_{V,p} = 0$, which implies isochoric plastic flow. The inelastic volumetric response is later added through a bulking variable ΔP. The current bulking formulation in the JH material models is explicit in nature, giving rise to step size dependence of the material models.

The JH2 material model with dilatation

An alternative to using the JH bulking formulation is to include volumetric plastic deformation (dilatation) through the plastic potential function. This allows implicit implementation of the material model. The plastic potential function from Equation 3 may be modified to

$$g(I_1, J_2, D) = \sigma_{eq}(J_2) - \psi\sigma_y(I_1, D), \qquad \textbf{Equation 4}$$

in which a scalar value $\psi \in \mathbb{R}$ can be used to scale the dependence on σ_y and thus I_1. For $\psi = 0$ the original (isochoric) formulation is retrieved, $\psi \neq 0$ results in plastic volumetric deformation with associated plasticity for $\psi = 1$. In a fully implicit algorithm this potential function removes the step size dependence while maintaining the dilatation (or bulking) effect found in the original JH material models.

It could be argued that dilatation effects reduce with increasing damage, and may even be absent for fully damaged material [9]. The plastic potential function can be modified to include dilatation by

$$g_I(I_1, J_2, D) = \sigma_{eq}(J_2) - \psi\,(1 - D)\sigma_i\ (I_1). \qquad \textbf{Equation 5}$$

Results

A unit test was performed on a four node quadrilateral element, using a 1 point Gauss integration scheme. All but one side was constrained in normal direction, the remaining side was displaced. Initially this surface was displaced in vertical direction to induce a compressive state. The compression was continued until maximum deformation δ_{max} was reached, after which the loading direction was reversed to regain the original configuration. The unit test performed under displacement control is depicted on the left in Figure 1.

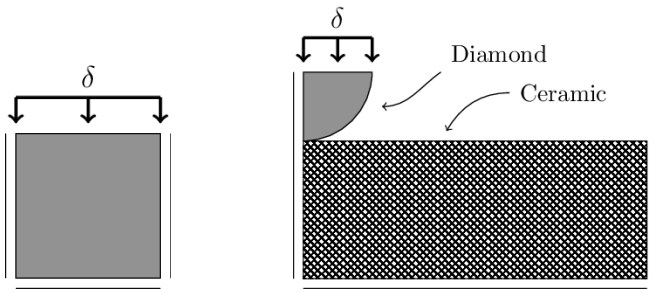

Figure 1: Left shows unit test set-up, right shows Brinell indentation test set-up

The JH2 model with the same parameters as described in the original paper [2] was used. Two simulations were performed, one with the original JH bulking, another with the plastic potential as described by Equation 5 using $\psi = 1.4$. Figure 2 shows the results of this unit tests. The unit test starts with undamaged material in a zero deformation and zero stress state. The left graph of Figure 2 shows the equivalent stress and pressure results. Elastic loading is observed from the origin to (A), after which the material strength (σ_{eq}) is found to gradually reduce from an intact to residual strength ($A \rightarrow B$). After the material has fully failed at (B) the pressure still increase as δ_{max} has not yet been reached. Unloading of the unit cube is initially elastic, until the material is plastically deformed in the reverse direction. The right graph in Figure 2 shows the pressure-volumetric deformation response, where the parameter $\mu = -\epsilon_V$ is a measure of volumetric deformation. A non-linear volumetric response ($A \rightarrow B$) can be observed while the material strength is gradually reducing. The volumetric response is also found to be inelastic since $P \neq 0$ after returning to the original configuration $\mu = 0.0$ at (C). From the graphs it can be found that, using the plastic potential from Equation 5, deviatoric and hydrostatic behaviour similar to the original JH2 model may be obtained.

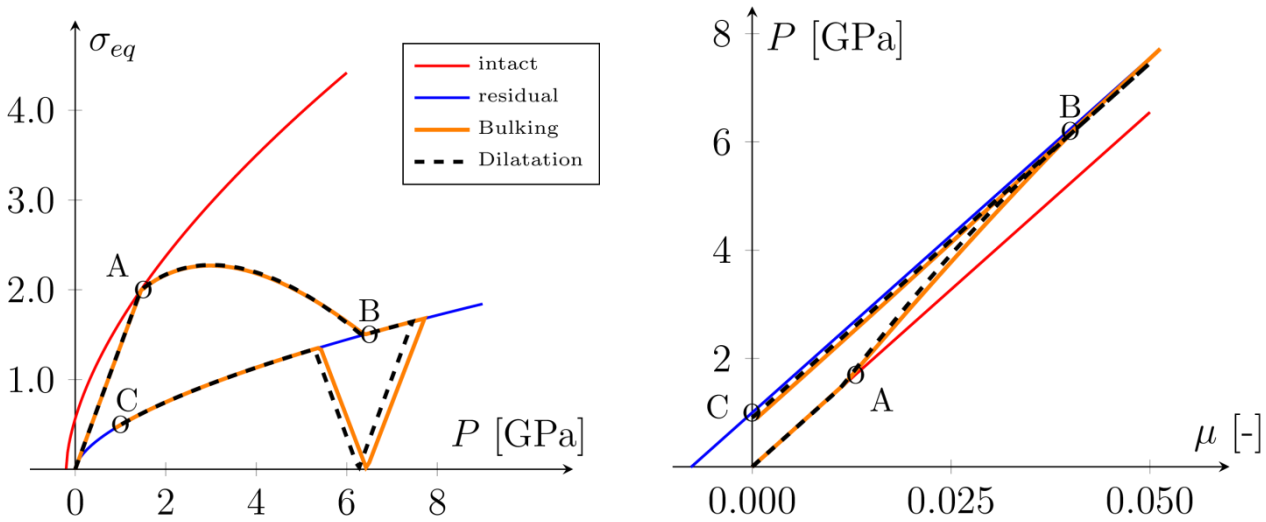

Figure 2: Unit test for the JH2 material model with bulking and a modified plastic potential function. Results for (l) the material strength and (r) the volumetric response are shown.

A Brinell indentation test was simulated on a four node quadrilateral element mesh, using a 2 by 2 Gauss integration scheme. A ceramic target was modelled as a disk with a thickness of 6 mm and a radius of 25 mm. The bottom edge of the ceramic was constrained in vertical direction. The indentor was modelled as a half sphere with a radius of 2 mm. A displacement is enforced on the top surface of the indentor to control the simulation. The top surface was displaced 25 μm in vertical direction, after which the indentor was retracted to its original position. For both parts horizontal displacements were constrained along the axis of revolution. The test setup can be seen on the right in Figure 1.

The JH material properties for the ceramic are similar to those in the unit test, but $\mu_{HEL} = 0.026$ and the elastic properties were chosen to represent Alumina with $E = 375$ GPa, $\nu = 0.24$. The spherical diamond indentor was modelled as a linear elastic material with $E = 1140$ GPa and $\nu = 0.07$. Contact between the two materials was described by a stick-slip penalty formulation with a coefficient of friction $\mu = 0.5$.

Figure 3 presents the load displacement data for the indentation simulations, three dilatancy cases are considered with $\psi = 0.0, \psi = 0.5$ and $\psi = 1.0$. Three observations follow from the figure. First, the indentation force is found to have a positive trend with the value of ψ. This is to be expected, as the plastically deformed material poses an additional pressure on the surrounding intact material. Second, permanent deformation after indentation has a negative relation with the value of ψ. This can also be related to an increase in pressure, where a higher pressure leads to a higher material strength in the JH2 material model and will thus lead to less plastic deformation. Third, energy dissipation measured by the area between the loading and unloading curves is also found to have a negative relation with ψ. Again the reduction in plastic deformation for the higher pressures and strengths explains the difference.

The equivalent plastic strain $\bar{\epsilon}_{eq}$ provides information on the ceramic failure behaviour during indentation. Figure 4 shows $\bar{\epsilon}_{eq}$ at the maximum indentation depth and Figure 5 after one indentation cycle, all figures use the same colour scheme, where green indicates $\bar{\epsilon}_{eq} > 10^{-4}$, yellow indicates $\bar{\epsilon}_{eq} > 10^{-3}$, while the highest equivalent plastic strains $\bar{\epsilon}_{eq} > 10^{-2}$ are found in the red zones. A spherical quasi-plastic zone can be found to appear slightly below the ceramic surface, in accordance with experimental results [6]. It is observed that the total plastically deformed zone increases in size for increased dilatation. However, the red zone with the maximum equivalent plastic strain is found to reduce. Another interesting observation is the behaviour at the surface. For low dilatation multiple locations are found where tensile failure occurs at the surface. This agrees well with [10], where dilatation is shown to suppress cone crack formation. The plastic deformation at the surface is also found to change during unloading, which indicates that additional damage occurs during this phase of the indentation. Capturing this damage under unloading may be important for dynamic material models, as unloading may occur due to stress wave propagation and reflection in an armour system.

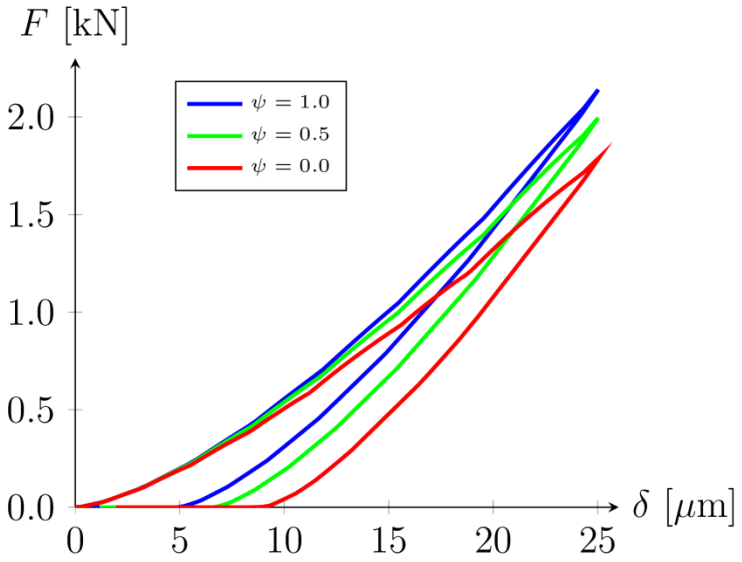

Figure 3: Brinell indentation test force displacement graph. The JH2 material model with dilatation is used. Three different values of ψ are used.

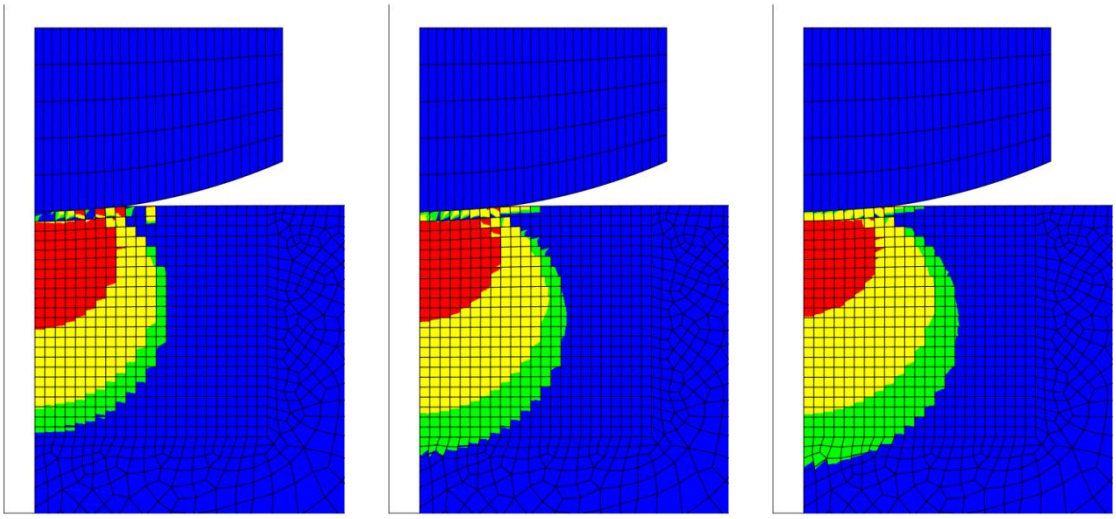

Figure 4: Equivalent plastic strain at maximum indentation δ_{max}. The JH2 material model with the plastic potential function from Equation 5 was used. From left to right $\psi = 0.0$, $\psi = 0.5$ and $\psi = 1.0$.

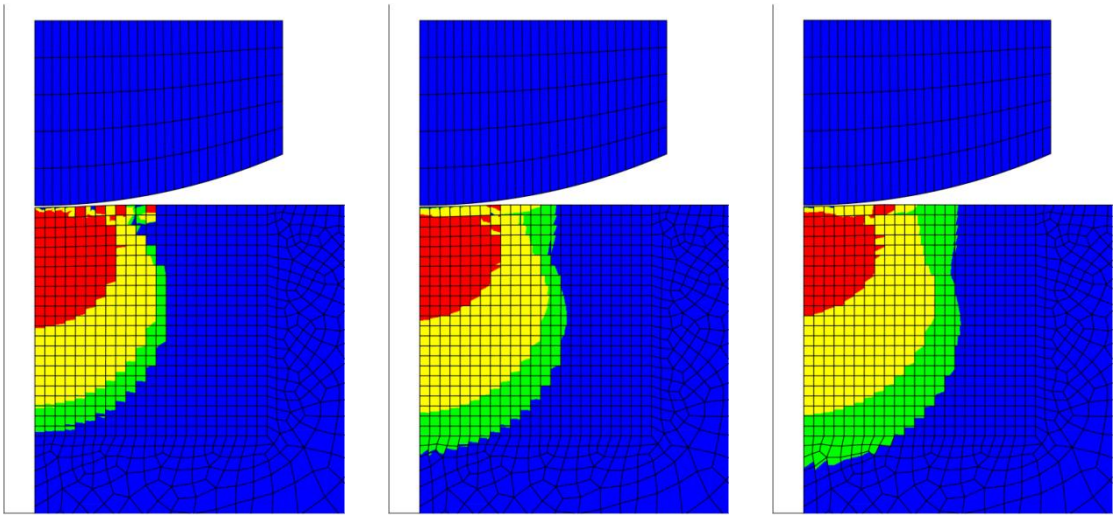

Figure 5: Equivalent plastic strain after one indentation cycle. The JH2 material model with the plastic potential function from Equation 5 was used. From left to right $\psi = 0.0$, $\psi = 0.5$ and $\psi = 1.0$.

To study localization and mesh-dependence, a mesh refinement study is performed. The same material parameters and test set-up were used as for the previous full indentation results. Four meshes were considered, the same mesh as before, one coarser mesh and two finer meshes. The resulting equivalent plastic strain at maximum indentation is shown in Figure 6. It can be seen that the semi-spherical plastic zone appears in each of the four meshes, all with a similar size. This result is expected, as the increasing strength with increasing pressure reduces the softening effect and may even lead to a behaviour similar to hardening plasticity. The behaviour under tension is, however, very different for all four cases. The position and number of elements failing under tension at the surface change upon refinement. The finest two meshes show a cone crack forming, although both appear in a different location. This may pose severe problems when ballistic problems are considered. For ballistic loading the cone cracks propagate and may eventually lead to catastrophic failure. A correct prediction of these cone cracks in the initial phases may therefore lead to more accurate results, even for dynamic ballistic simulations. Based on the current results it is found that mesh-dependence exists upon tensile failure.

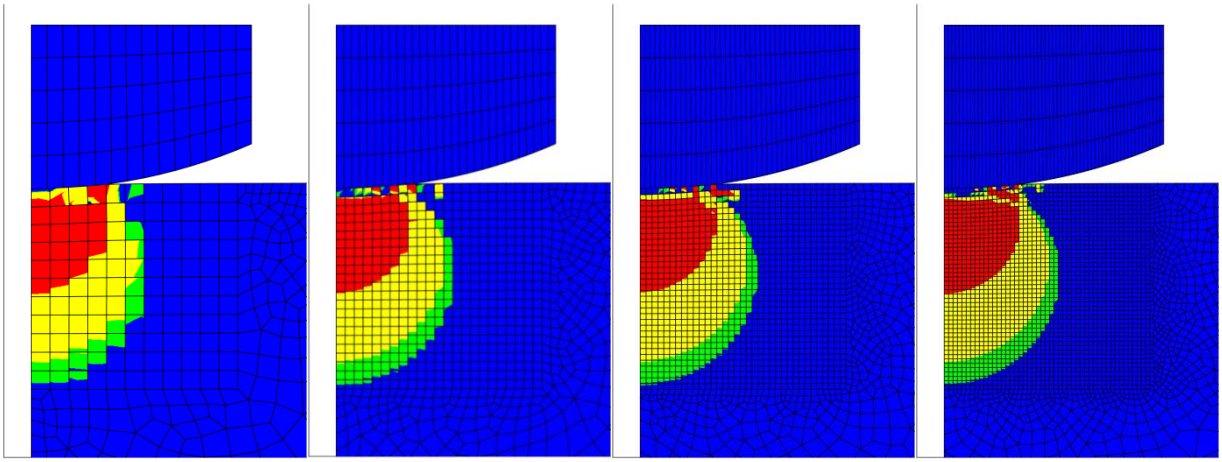

Figure 6: Indentation test mesh refinement study. Equivalent plastic strain at maximum indentation δ_{max}. JH2 material model is used with $\psi = 0.0$.

Conclusions

It has been shown that a plastic potential function can be used to obtain dilatational behaviour in a FEM simulation. For simple unit tests dilatation was found to give results similar to the JH2 model with bulking. More complex indentation tests revealed a relation between the amount of dilatation and indentation force, energy dissipation and surface tensile failure. Damage for ceramics under indentation was found to grow in both the loading and the unloading phase, where mainly shallow subsurface damage was found during the unloading phase. Dilatation was furthermore seen to affect cone crack formation during indentation. The mesh-refinement study showed that the behaviour of the current material model under tension leads to mesh dependent results.

References

1. G.R. Johnson and T.J. Holmquist. 1992. A Computational Constitutive Model for Brittle Materials Subjected to Large Strains. *Shock Wave and High-Strain-Rate Phenom. Mater.* 1075-1081.
2. G.R. Johnson and T.J. Holmquist. 1994. An Improved Computational Constitutive Model for Brittle Materials. *API Conf. Proc.* **309**, 981-984.
3. G.R. Johnson, T.J. Holmquist and S.R. Beissel. 2003. Response of Aluminum Nitride (Including a Phase Change) to Large Strains, High Strain Rates, and High Pressures. *J. Appl. Phys.* **94**, 1639-1646. (10.1063/1.1589177)
4. E.A.N. Gamble, B.G. Compton, V.S. Deshpande, A.G. Evans and F.W. Zok. 2011. Damage Development in an Armor Ceramic Under Quasi-Static Indentation. *J. Am. Ceram. Soc.* **94**, s204-s214. (10.1111/j.1551-2916.2011.04472.x)
5. T.J. Holmquist and A.A. Wereszczak. 2010. Using Hertzian Indentation to Understand the Strength and Ballistic Resistance of Silicon Carbide. *Int. J. Appl. Ceram. Tech.* **7**, 625-634. (10.1111/j.1744-7402.2010.02540.x)
6. B. Lawn. 1998. Indentation of Ceramics with Spheres: A Century after Hertz. *J. Am. Ceram. Soc.* **81**, 1977-1994. (10.1111/j.1151-2916.1998.tb02580.x)
7. P. Wriggers, T. Vu Van and E. Stein. 1990. Finite Element Formulation of Large Deformation Impact-Contact Problems with Friction. *Comput. Struct.* **37**, 319-331. (10.1016/0045-7949(90)90324-U)
8. M.A. Crisfield. 1991. Non-Linear Finite Element Analysis of Solids and Structures: Essentials. (ISBN-13: 978-0471970590)
9. D. Fernández-Fdz, R. Zaera and J. Fernández-Sáez. 2011. A Constitutive Equation for Ceramic Materials used in Lightweight Armors. *Comput. Struct.* **89**, 2316-2324. (10.1016/j.compstruc.2011.08.003)
10. J.C. Lasalvia and J.W. McCauley. 2010. Inelastic Deformation Mechanisms and Damage in Structural Ceramics Subjected to High-Velocity Impact. *Int. J. Appl. Ceram. Tech.* **7**, 595-605. (10.1111/j.1744-7402.2010.02489.x)